

## Inclusion of Aeroelastic Twist into the CFD Analysis of the Twin-Engine NASA Common Research Model

Scott. Eberhardt<sup>1</sup>, Kent Benedict<sup>2</sup>, Linda Hedges<sup>3</sup>, Anna Robinson<sup>4</sup>  
 Edward N. Tinoco<sup>5</sup>

### Abstract

**The Fifth AIAA CFD Drag Prediction Workshop tasked attendees with generating aerodynamic data for the NASA Common Research Model wing-body configuration. Numerical calculations were performed on a set of standardized grids, categorized by the level of grid refinement. These grids represented the "as-built" model and did not include any anticipated test related aero-elastic deformation. Because of this, numerical analyses presented at the Fifth Drag Prediction Workshop showed excessive discrepancies when compared to wind tunnel data. These issues have prompted this work, which aims to examine the contribution of steady-state aero-elastic deformation to the numerical solution accuracy for the NASA Common Research Model. Numerical analysis results for the deformed geometry are compared to experimental data and "as built" solutions. Results show a better match for lift and wing-section "rooftop" pressures.**

### I. Introduction

Beginning in 2001 a roughly biannual effort has been undertaken to assess the status of computational fluid dynamics (CFD) simulations for computing drag on complex aircraft geometries. The first Drag Prediction Workshop (DPW) set the tone for an open, impartial forum to evaluate the state-of-the-art CFD tools. Over the next four workshops this model has continued and the complexity of the geometries has continued to increase. For each workshop, wind tunnel data was collected for a transport configuration in various wind tunnel facilities. The goal was not necessarily to match the wind tunnel data with the CFD tools, but to understand and account for the differences. This paper discusses a step in reconciling the wind tunnel data with two CFD analysis tools by including aerodynamic twist and bending into the analysis.

Effective use of computational fluid dynamics (CFD) is a key ingredient in successful design of modern commercial aircraft. The combined pressures of market competitiveness, dedication to the highest of safety standards, and desire to remain a profitable business enterprise all contribute to make intelligent, extensive, and careful use of CFD a major strategy for product development capable of revolutionizing the process of aerodynamic design. CFD has joined the wind tunnel and flight test as primary tools of the trade<sup>1,2,3,4</sup>; each has its strengths and limitations. Because of the tremendous cost involved (and potential risk) in flight testing, modern aircraft development places major focus on the use of CFD and the wind tunnel prior to flight. The wind tunnel is best suited for validation and database building within acceptable limits of a development program's cost and schedule. Historically, CFD has been considered unsuited for such a task. However, the wind tunnel typically does not produce data at flight Reynolds number, is subject to sometime significant wall and mounting system corrections, and is not well suited to provide flow details. The strength of CFD is its ability to quickly produce a small number of simulations leading to the understanding necessary for design. Of great utility in this connection is the fact that CFD can be used in an "inverse design" or optimization mode, predicting the necessary geometry shape changes to optimize certain flow characteristics or a payoff function (e.g., drag). Beyond this payoff, CFD is heavily used to provide corrections for the extrapolation of data acquired experimentally (typically from testing a reduced-scale model of the vehicle in a wind tunnel) to conditions that characterize the full-scale flight vehicle.

<sup>1</sup> Chief Engineer, Stark Aerospace, Inc. Analytical Methods Division, USA, Associate Fellow

<sup>2</sup> Engineer, Stark Aerospace, Inc. Analytical Methods Division, USA, Member

<sup>3</sup> President, Stark Aerospace, Inc. Analytical Methods Division, USA

<sup>4</sup> Engineer, Stark Aerospace, Inc. Analytical Methods Division, USA

<sup>5</sup> The Boeing Company, Retired, Associate Fellow

Finally, CFD is used to provide understanding and insight as to the source of undesirable flight characteristics, whether they are observed in subscale model testing or in the full-scale flight-testing. Collectively, flight test, wind tunnel testing, and CFD all contribute to minimizing risk and uncertainty in a new airplane product.

Before committing to the use of CFD, it must make economic sense. Essential elements to delivering this confidence have previously been described in Reference 1. One key element is the on-going process of CFD validation. Is the CFD “close enough?” In assessing the accuracy of CFD, wind tunnel results are frequently used as the “gold standard.” However, even if we had the perfect CFD code we would not, nor should we get, perfect agreement with wind tunnel results because the wind tunnel has its own imperfections which also must be understood, or at least recognized, in order to assess or validate the CFD. Effective CFD validation requires intimate knowledge of both the CFD and the experimental data being compared. CFD validation cannot consist of the comparison of the results of one code to those of one experiment. Rather it is the agglomeration of comparisons at multiple conditions, code-to-code comparisons, an understanding of the wind tunnel corrections, etc., that leads to the understanding of the CFD uncertainty and validation of its use as an engineering tool<sup>2</sup>.

The Drag Prediction Workshops offer a forum where the agglomeration of comparisons and the understanding of CFD uncertainty and validation can take place. A Common Research Model (CRM) was built for DPW-IV, held in 2009. The goal of that workshop was “blind” predictions of lift and drag. Participants were asked to prepare solutions before wind tunnel data was released. One process developed was to produce standardized grids, in an attempt to make apples-to-apples comparisons of the tools. For the fifth Drag Prediction Workshop, held in June of 2012, the grids were supplied for the “as built” CRM. The simulations presented at the workshop greatly over-predicted the “rooftop” pressures aft of the wing leading edge, and over-predicted lift and lift slope. In this paper we will show comparisons between two CFD codes of differing physical approximation with wind tunnel test data for a commercial transport type configuration obtained for the 4<sup>th</sup> and 5<sup>th</sup> CFD Drag Prediction Workshops. An important consideration in making these comparisons will be to show the importance of accounting for the aeroelastic twist of the wind tunnel model wing under the varying test conditions.

### CFD Methods

Two CFD methods currently in use that meet the accuracy and usability criteria by the product development community were evaluated in this study. The methods chosen represented two levels of physical modeling:

VSAERO<sup>3</sup> is a subsonic panel method that has evolved over the past 30 years. The public domain version<sup>4</sup> was limited to external flow problems of 1000 panels or less. Version 7 has solved problems with 70 thousand panels. The code has been rewritten in the past 20 years based upon customer experience, with priority given to robustness, accuracy, versatility, speed and simplicity. Notable additions include: internal flows<sup>5</sup>, body wakes, added mass, non-uniform inflow, free surfaces<sup>6</sup>, warped panels<sup>7</sup>, boundary layer coupling, unstructured grids of triangular panels<sup>8</sup>, induced drag analysis<sup>9</sup>, and oscillatory flows<sup>10</sup>. VSAERO applications include: aircraft, cars, sailboats, ships, and wind turbines. Typical model sizes are 10-20 thousand panels with compute times of minutes on a desktop PC.

CFD++<sup>11</sup> is a commercial code that solves the Navier-Stokes equations on a hybrid-element unstructured grid. It uses an algebraic multigrid technique to accelerate convergence. The code allows for the use of various elements within the same mesh, including: hexahedral, triangular prism, pyramid and tetrahedral elements. The solver is based on a second-order accurate Total Variation Diminishing finite-volume scheme coupled with an implicit, backward-Euler time-stepping and multi-grid convergence acceleration. The preconditioned compressible equations are used for low-speed flows to accelerate convergence, particularly for external flows with free-stream Mach numbers of less than 0.5.

### Geometry Morphing

Twist and deflection were applied to the Common Research Model (CRM) wing geometry with AMI’s in-house tools. Experimental twist and deflection measurements were splined across the wing span at the 40% chord line to generate a smooth deformation schedule. The CRM surface geometry was morphed manually to match this defined twist schedule. The nacelle was rotated about the wing elastic axis as a rigid component to match the local deformation of the wing. The pylon was similarly rotated but also slightly deformed in order to maintain connectivity between the nacelle and wing. Bending about the X axis was performed in a similar fashion for the wing, nacelle, and pylon.

### The Wind Tunnel Model

The subject geometry is the Common Research Model (CRM)<sup>12</sup>, developed jointly by NASA's Subsonic Fixed Wing (SFW) Aerodynamics Technical Working Group (TWG) and the AIAA Drag Predictions Workshop Organizing Committee. The CRM is representative of a modern transonic commercial transport airplane, and was designed in the full configuration with a low wing, body, horizontal tail, and engine nacelles mounted below the wing. Pertinent geometric parameters are listed in Figure 1. For this paper, the wing-body and wing-body-pylon-nacelle configurations were analyzed. A rendering of the geometry is shown in Figure 1, along with a photo of the wind tunnel model installed in the NASA Ames 11ft Transonic Wind Tunnel. The CRM was the subject geometry for the 4<sup>th</sup> and 5<sup>th</sup> AIAA Drag Prediction Workshops<sup>13,14</sup>.

Table 1 - Reference Quantities for the CRM

$S_{ref}$	594,720.0 in <sup>2</sup>	= 4,130 ft <sup>2</sup>	[458.89 m <sup>2</sup> ]	$X_{ref}$	1,325.9 in	[33.68 m]
$S_{trap}$	576,000.0 in <sup>2</sup>	= 4,000 ft <sup>2</sup>	[444.44 m <sup>2</sup> ]	$Y_{ref}$	468.75 in	[11.91 m]
$b$	2,313.5 in	= 192.8 ft	[58.765 m]	$Z_{ref}$	177.95 in	[4.520 m]
$c_{ref}$	275.800 in	= 22.98 ft	[7.0053 m]	$\Lambda_{C/4}$	35.0°	
AR	9			$\lambda$	0.275	

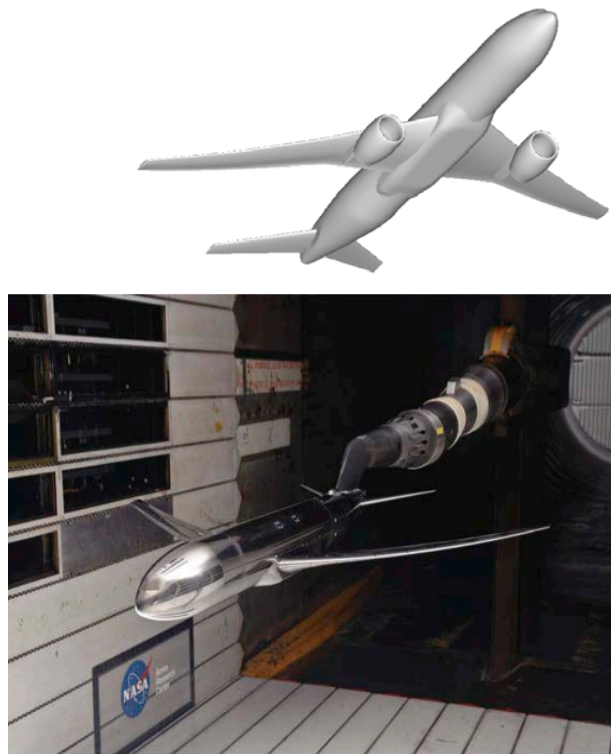


Figure 1 - NASA Common Research Model Geometry

An experimental investigation of the NASA Common Research Model was conducted both in the NASA Langley National Transonic Facility and NASA Ames 11-foot Transonic Wind Tunnel Facility. Data taken at these facilities included model forces and moments, wing pressures and wind tunnel model wing twist and deflections under various flow conditions. In spite of being built of high strength steel, the wing of a wind-tunnel model will deflect and twist under aerodynamic load. The measured twist along the

span of the wing is shown for several different angles of attack in Figure 2. In a study that demonstrated using a measured wing twist rather than the as-built model twist<sup>14</sup>, CFD analysis was based on just one twist distribution that corresponded to that at the “cruise” flight condition. This study will look at varying the twist distribution at each angle-of-attack analyzed. Ideally the solutions would be the result of coupled aerodynamic/structural aeroelastic calculations. In this case, however, measured twist increments will be used at each angle of attack analyzed. Either way a reliable process to modify the surface geometry inputs to the CFD analysis code is needed.

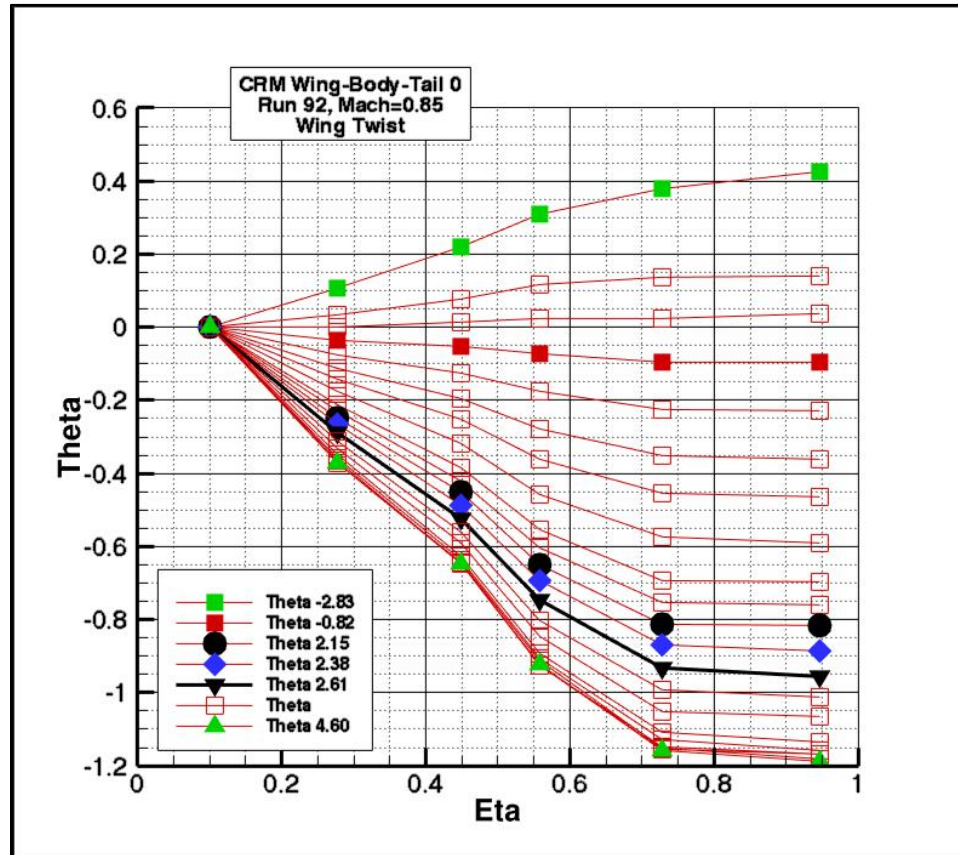


Figure 2: Measured twist along the span of the wing for various angles of attack

## II. Description of Computational Models and Method Used for Incorporating Twist

In-house grids were used for both VSAERO and CFD++ in order to function properly with the mesh generation and deformation processes in place.

### VSAERO Model

The CRM model consisting of a wing and body used in the analysis is shown in Figure 3. This model was gridded using structured (quadrilateral) grids on the wings and part of the body and unstructured (triangular) grids on the remaining body, with a total of 3 structured patches and 11 unstructured patches. The model consists of 4983 body panels and 1754 wake panels. Twist was applied to the geometry by linearly interpolating the twist schedule in the butline direction.

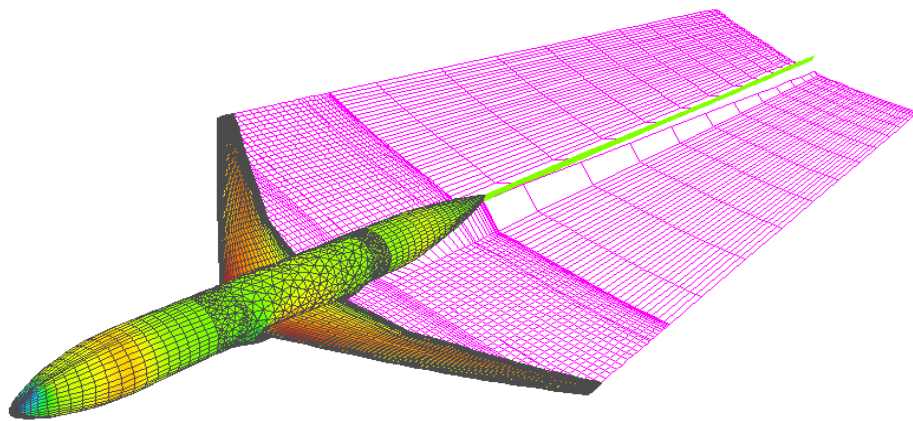


Figure 3 – CRM Wing-Body with VSAERO grid and wake

#### CFD++ Model

The CFD++ surface grids shown in Figures 4 & 5 are representative of the grids generated subsequent to the geometry deformations. The surface panel distribution was replicated for each rigid and morphed model in ANSA. The wing-body-tail grid has 95,000 panels on the wing and 23,000 on the fuselage and tail. The wing-body-nacelle-pylon mesh has 95,000 panels on the wing, 13,000 panels on the nacelle and pylon, and 20,000 panels on the fuselage. The wing surface grid was highly concentrated near regions of interest including the wing leading edge, trailing edge, tip, and root. A rectangular prism far field extending 10 body lengths in the X, positive Y, and Z directions was meshed with triangles. The flow field was then gridded as an unstructured hybrid mesh with the AFLR3 volume meshing tool. The wing-body-tail volume meshes contain approximately 10 million cells, and the wing-body-nacelle-pylon meshes contain approximately 11 million cells.

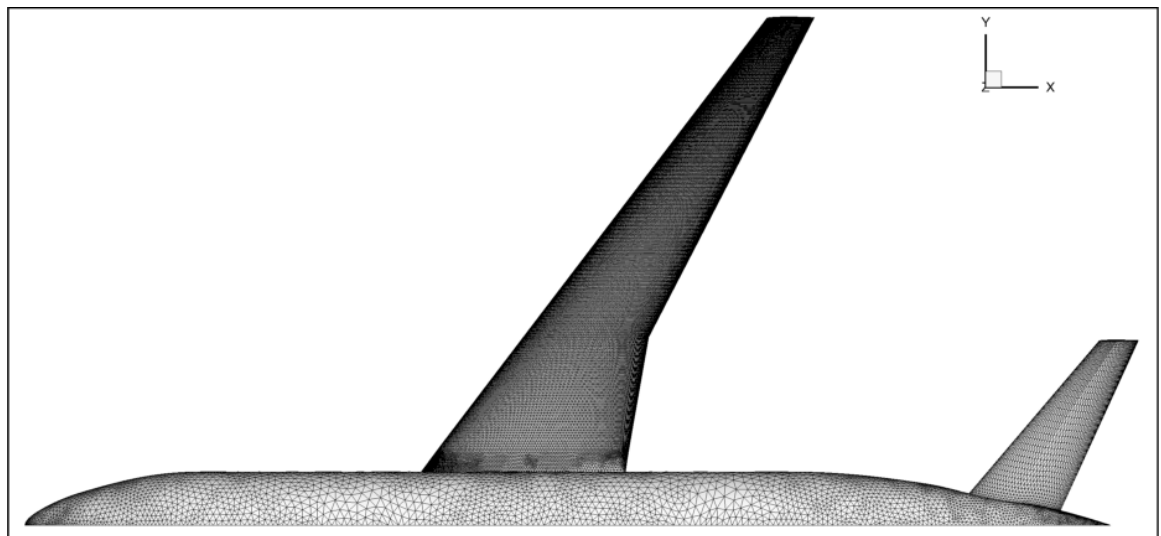


Figure 4 – CRM Wing-Body-Tail ANSA surface grid top view

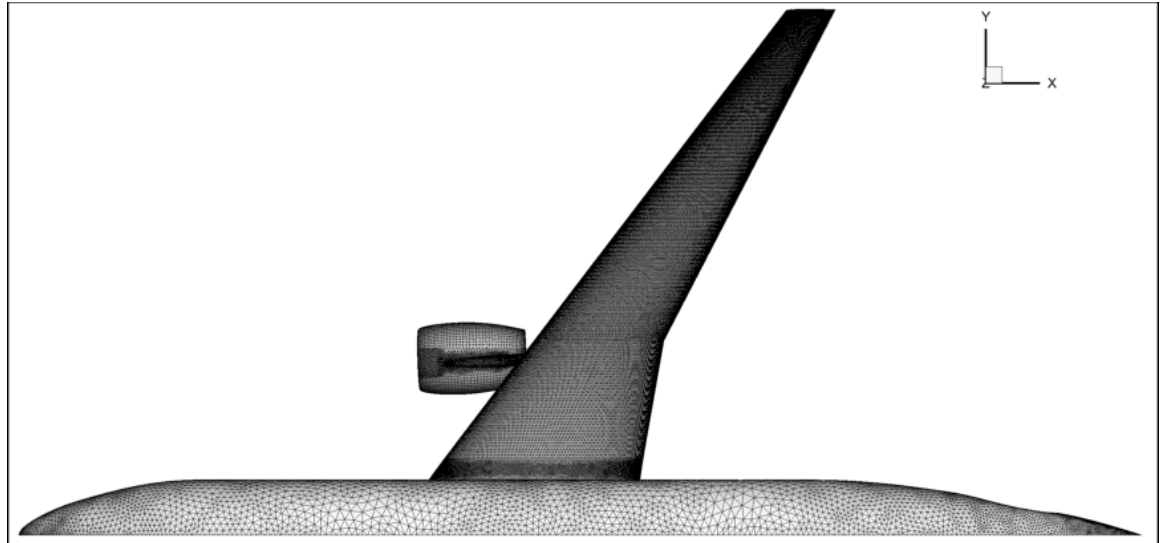


Figure 5 – CRM Wing-Body-Tail-Nacelle-Pylon ANSA surface grid top view

### III. Computational Results

#### VSAERO Results

Two sets of analyses of the CRM model were obtained through VSAERO. Preliminary work with VSAERO was presented at the 5<sup>th</sup> ANSA and  $\mu$ ETA International Conference<sup>15,16</sup> and is shown here for completion. The first set consisted of analysis of the CRM at several angles of attack using the fixed geometry used for the Drag Prediction Workshop. The second set consisted of analysis of the CRM at several angles of attack using the measured wing twist distribution for each angle. The twist angles were taken from NASA's experimental data and applied to the geometry data using a 1<sup>st</sup> degree interpolation. Lift and pitching moment results for the two sets of analyses are shown in Figure 6 and Figure 7. As indicated in Reference 17, the wind tunnel data is subject to significant wind tunnel wall and mounting system interference and is not fully representative of "free-air". CFD results presented at the 5<sup>th</sup> Drag Prediction Workshop<sup>18</sup> differed from the test data an average of approximately 0.5 degree in angle of attack for a given lift, and 0.05 in pitching moment coefficient. These increments were applied to the VSAERO results as uniform tares to angle of attack and pitching moment. The resulting VSAERO results show improved agreement with test data with the inclusion of aeroelastic twist in the CFD model.

The effects of including the aeroelastic twist in the solutions is most evident in the distribution of section lift coefficient along the span of the wing. This is illustrated in Figure 8 in which the wing section lift coefficient is plotted vs. the wing span fraction for both the fixed twist and the aero twist at the same angle of attack. The effect of the aeroelastic twist is to reduce the lift on the outboard portion of the wing. The experimental data has not been processed to yield the section force and moment characteristics, hence there is no experimental data with which to compare.

#### CFD++ Results

As in the case of the VSAERO analyses, two sets of analyses of two CRM models were performed using the Navier-Stokes code, CFD++. The first set consisted of analysis of the CRM at several angles of attack using the "Rigid As-Built" wing/body/tail and the wing/body/nacelle geometries defined for both the 4<sup>th</sup> and 5<sup>th</sup> AIAA Drag Prediction Workshop. The second set consisted of analysis of the two CRM geometries at several angles of attack using the measured wing twist distribution for each angle. These solutions are referred to as "Aero Twist."

#### CRM Wing-Body-Tail

The first results will be for the wing/body/tail configuration, as shown in Figure 9. A simple plot of  $C_p$  is illustrated at Mach 0.85 and a  $CL$  of 0.5, which represent the assumed design point for the aircraft. Note that all the CFD++ transonic calculations were done at Mach 0.85.

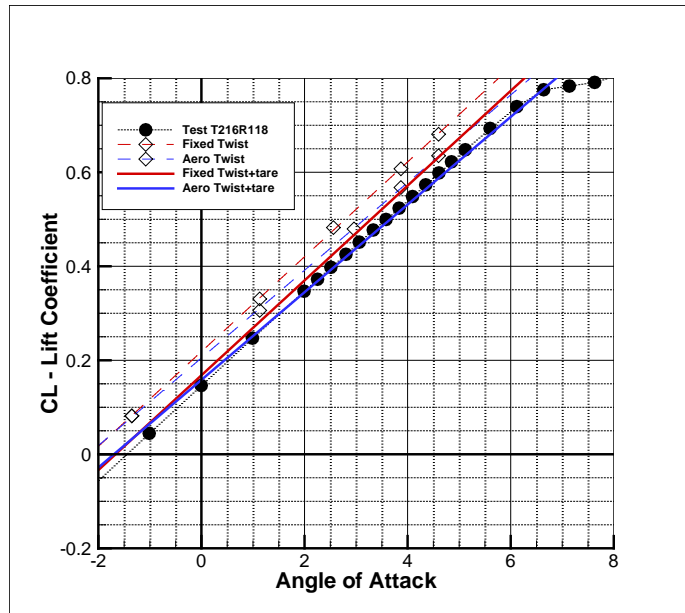


Figure 6 – CRM wing-body: angle of attack vs lift coefficient

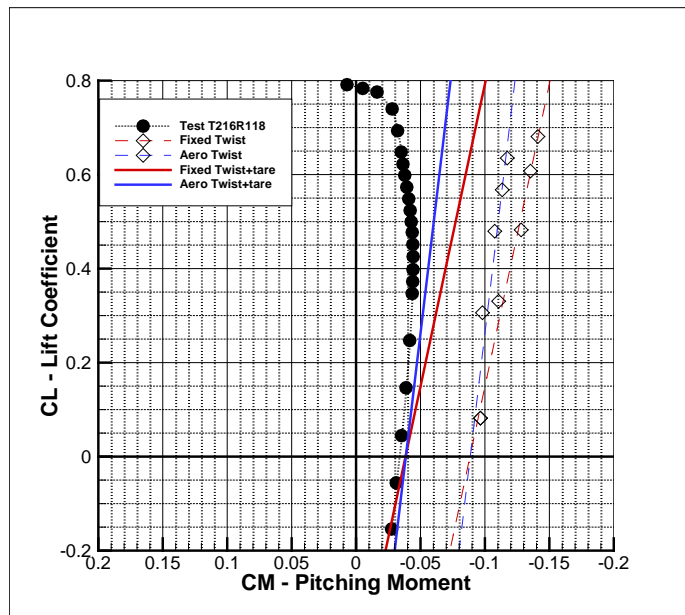


Figure 7 – CRM wing-body: pitching moment versus lift coefficient

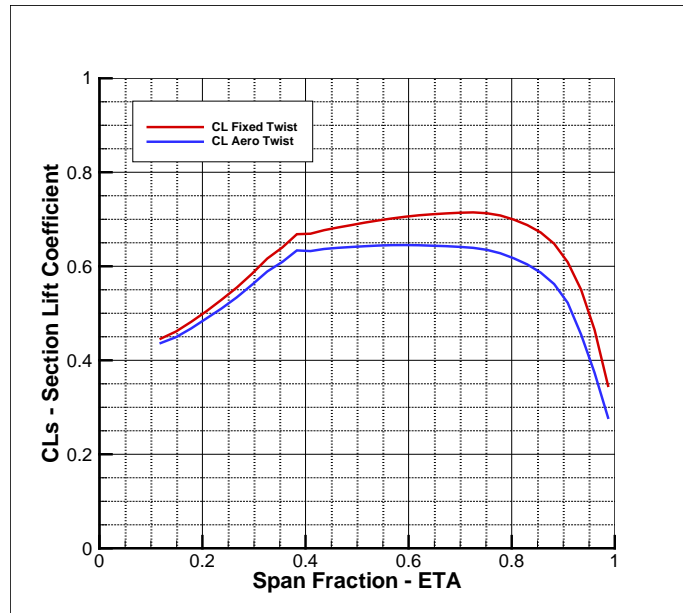


Figure 8 – CRM wing-body: section lift coefficient vs. wing span fraction.

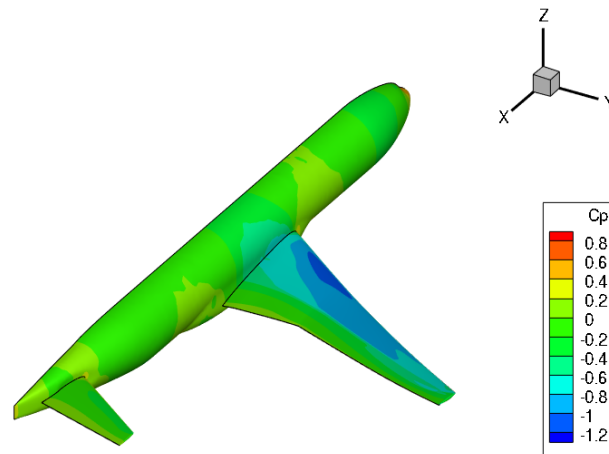


Figure 9. CRM Wing-Body-Tail Configuration, Mach=0.85, CL=0.5

Figure 10 is a plot of the twist angles used for the “Aero Twist” calculations. The twist angles were taken from NASA’s experimental data and applied to the geometry data as described in the introduction.

Lift and pitching moment results for the two sets of analyses are shown in Figure 11. As previously indicated<sup>15</sup> the wind tunnel data is subject to significant wind tunnel wall and mounting system interference and is not fully representative of “free-air”. A description of the corrections applied to the wind tunnel data and most of the data can be found in Reference 18. CFD analyses typically consider only the “free-air” configuration without the wind tunnel. The resulting CFD++ results show improved agreement with the test data with the inclusion of the aeroelastic twist in the CFD model. Further improvement in the correlation with experimental data is seen when the effect of the upper swept strut mounting system is added to the “free-air” CFD results. These “sting” corrections were obtained from the studies described in Reference 17. The computational model with the sting used in that study is illustrated in Figure 12. The effect of the upper swept strut mounting system is to reduce lift at a given angle-of-

attack and to make the pitching moment more positive. The effect of the aeroelastic twist is to reduce the lift curve slope (CL vs. angle-of-attack) and to reduce the stability (dCM/dCL).

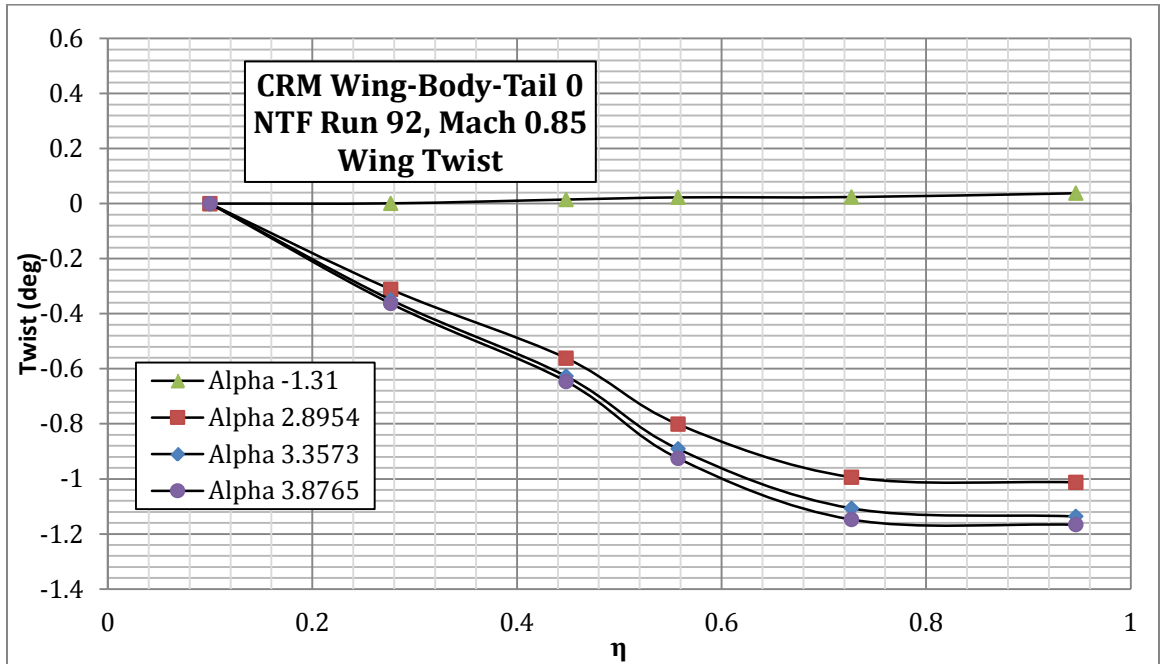


Figure 10. Wing Twist Angles Applied to CRM Wing at Various Angles-of-Attack

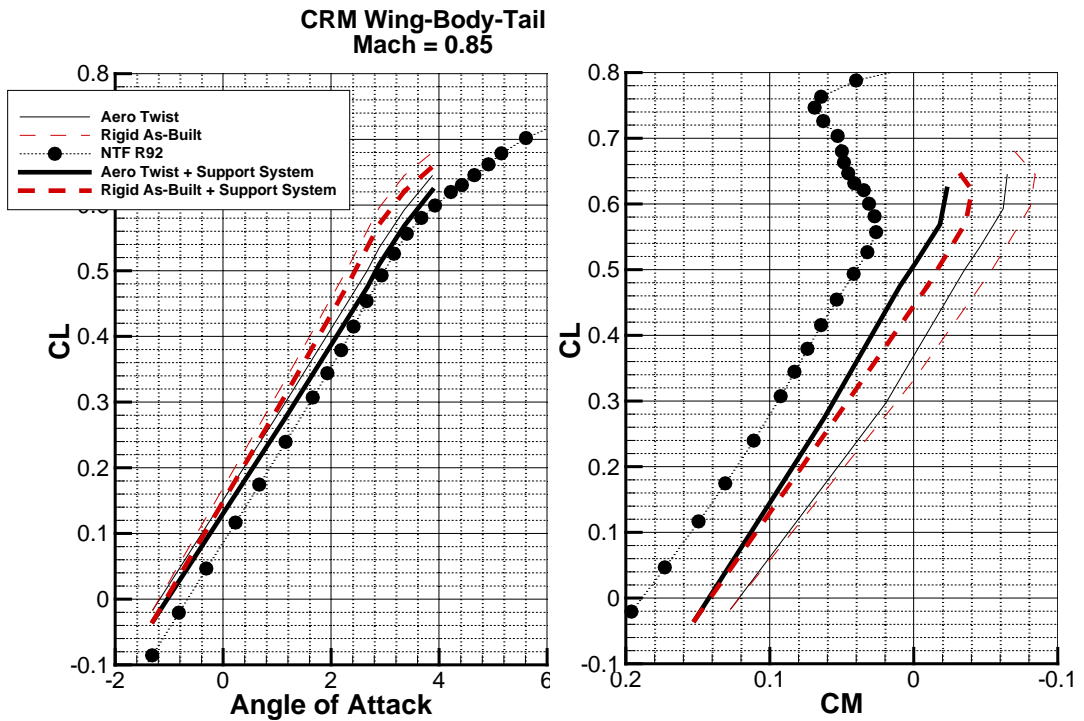


Figure 11 – Lift and Pitching Moment Comparison with Test Data

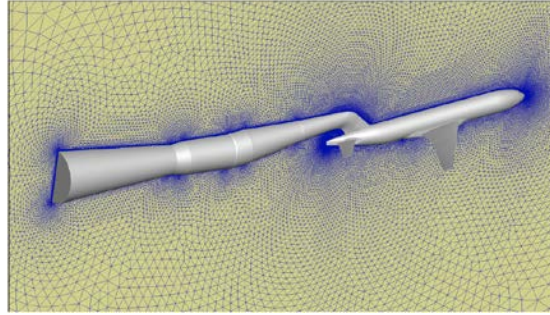


Figure 12 – CFD Model with Upper Swept Sting/Strut from Reference 15

The effects of wing aeroelasticity can be easily seen in the wing pressure distributions comparisons. A comparison of computed results with experimental data at four spanwise stations is shown in Figures 13 to 16 for four angles of attack. Note that lift coefficients shown for the CFD results do not include the upper swept sting/strut correction. This would reduce the CFD lift coefficients by approximately 0.025. Figure 13 shows results for an angle-of-attack of -1.31 degrees. At this angle of attack the aeroelastic twist as shown in Figure 10 is essentially zero. The Aero Twist and Rigid As-Built solutions are identical. The agreement of CFD with test data is very good.

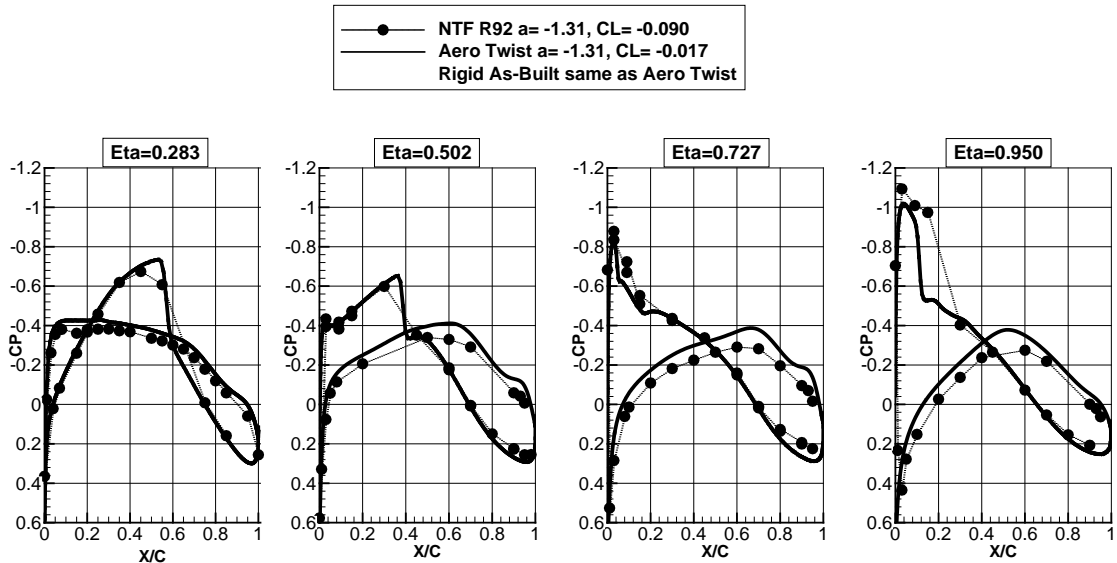


Figure 13. Wing Pressure Distribution Comparison at Angle of Attack = -1.31 degrees.

Figure 14 shows results for angle-of-attack of 2.90 degrees. Here CFD results with the Aero Twist for this angle of attack are shown matching angle of attack and results matching lift coefficient. CFD results with the Rigid As-Built twist are shown matching angle of attack. At the inboard station,  $\eta=0.283$  there is little aeroelastic twist and little difference in the CFD results. Moving outboard the effects of the aeroelastic twist becomes much more significant. The Rigid As-Built solution predicts a too negative pressure coefficient on the upper surface. This is often referred to as predicting too high a “rooftop” pressure. The Aero Twist solutions are in much better agreement with the test data. Of particular importance is the proper prediction of the “rooftop” pressure levels. The prediction of too negative a pressure level at  $\eta=0.95$  is indicative of the aeroelastic twist actually being greater than indicated by the published data.

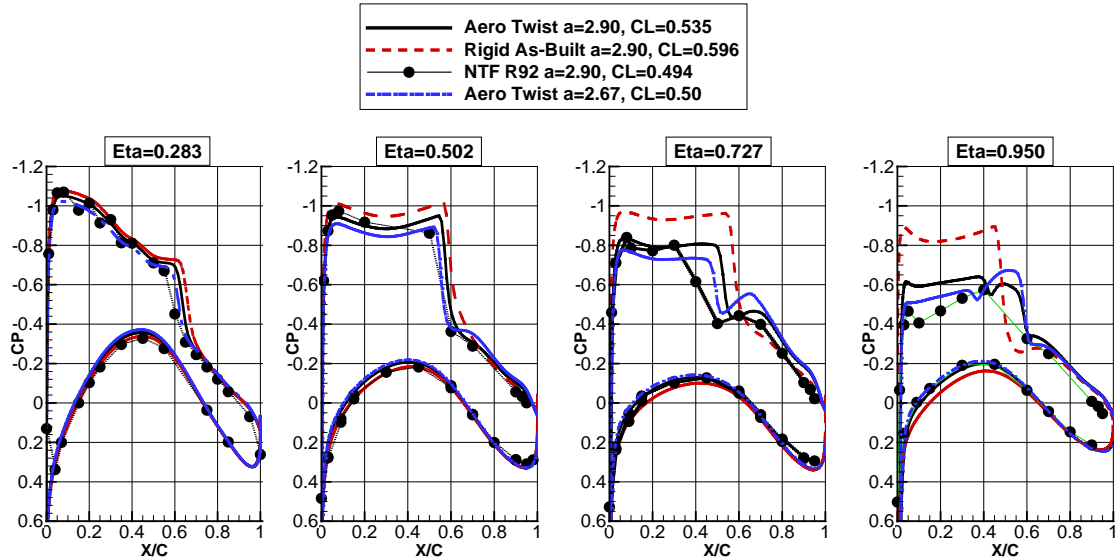


Figure 14. Wing Pressure Distribution Comparison at Angle of Attack = 2.90 degrees.

Figures 15 and 16 show comparisons for angle of attack of 3.36 and 3.88 degrees. Aero Twist and Rigid As-Built CFD results matching angle of attack are shown compared with experimental data. As seen in Figure 14 there is little difference in the CFD results at spanwise station  $\eta=0.283$ . Further outboard at  $\eta=0.502$  and  $0.727$  the Aero Twist results match the “rooftop” pressure levels very well while the Rigid As-Built results predict much too negative values. The  $\eta=0.95$  comparisons suggest that greater aeroelastic twist was probably called for. Remember that for the Aero Twist solutions, a different spanwise twist distribution is specified for each angle of attack.

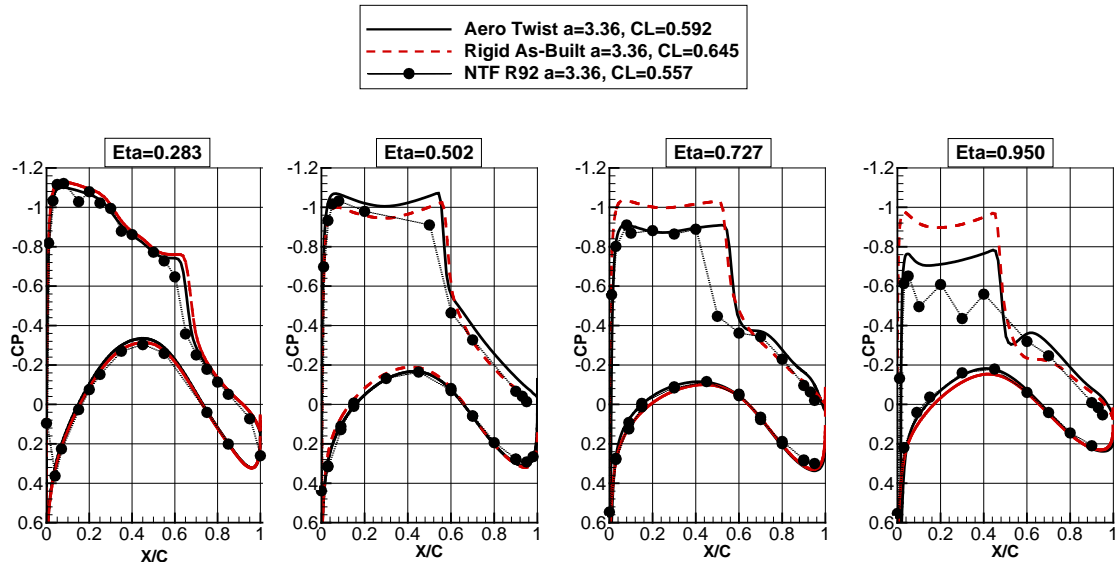


Figure 15. Wing Pressure Distribution Comparison at Angle of Attack = 3.36 degrees.

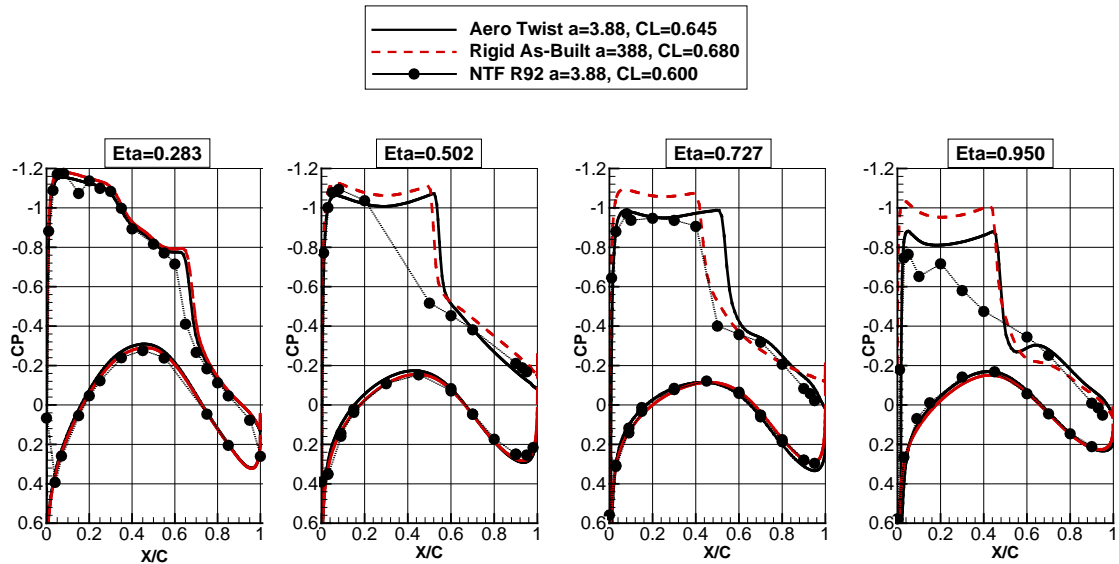


Figure 16. Wing Pressure Distribution Comparison at Angle of Attack = 3.88 degrees.

Another way to look at the effect of wing aeroelasticity is to look at the distribution of wing section lift coefficient across the span of the wing. Figure 17 shows the comparison of section lift across the span for Aero Twist and Rigid As-Built solutions with experimental data at an angle-of-attack of 2.90 degrees. Shown in Figure 14 are two Aero Twist solutions; one matching angle-of-attack, the other matching lift coefficient. This clearly shows that the Rigid As-Built solution predicts too high a lift distribution on the outboard part of the wing. This may also imply that the actual aeroelastic twist may have been greater than that used in the CFD solutions.

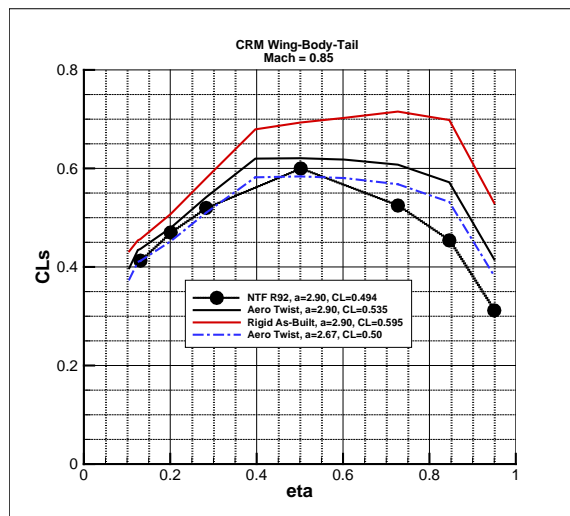


Figure 17. Spanwise Lift Coefficient Distribution Comparison at Angle-of-Attack = 2.90 degrees

Wing structural aerodynamic loads and the resulting structural weight is highly influenced by the variation of section lift as a function of angle-of-attack across the wing span fraction, eta. Section lift coefficient as a function of angle of attack is shown at three different spanwise locations in Figure 18. As expected, the effects of aeroelasticity are most evident at the outboard stations. Note that the effect of aeroelasticity is to reduce the section lift curve slope (CLs vs. angle of attack). Although there is a lift level difference, the section lift curve slope is well predicted by the Aero Twist results. Keep in mind that while the change in slope at the outboard stations is already significant for this wind tunnel model, we can expect

the reduction to be even greater for aeroelastics of a real airplane structure. Proper accounting for the airplane wing aeroelastics can significantly reduce the design loads and the resulting wing weight. Improper accounting can result in a higher weight and the resulting loss of aircraft performance, or worse yet, and understrength wing and an un-certifiable airplane in need of an expensive redesign.

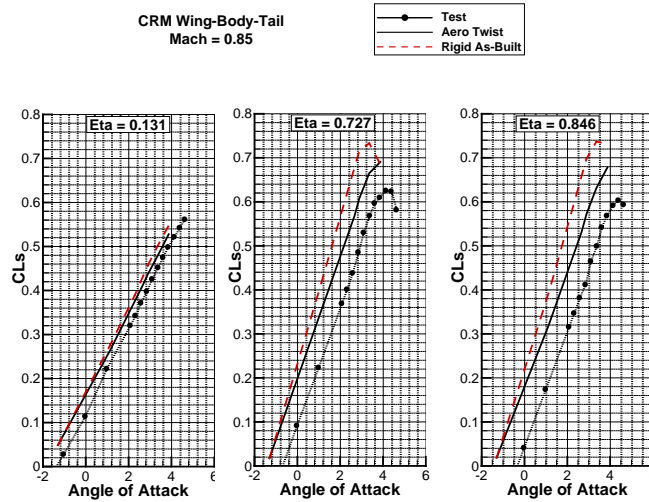


Figure 18. Section Lift vs. Angle of Attack

To better understand the differences in section lift as angle of attack is increased, pressure distributions at the three spanwise fractions are shown in Figures 19 to 21. CFD Aero Twist and Rigid As-Built solutions are compared with experimental data. Figure 19 shows results for four angles of attack at the inboard most station,  $\eta=0.131$ . Little difference is seen between the two CFD solutions and experimental data. Further out board at  $\eta=0.727$  and  $\eta=0.846$ , shown in Figures 20 and 21, the difference between the Aero Twist and Rigid As-Built solutions is quite evident. Note that the “rooftop” pressure level is well predicted by the Aero Twist solutions. Also evident is one of the primary reasons for the higher lift levels of the CFD solutions compared the experimental data; the prediction of a further aft shock location and higher aft loading. The reason for this is not known, but is similar to most solutions submitted to the 5<sup>th</sup> AIAA Drag Prediction Workshop<sup>14</sup>.

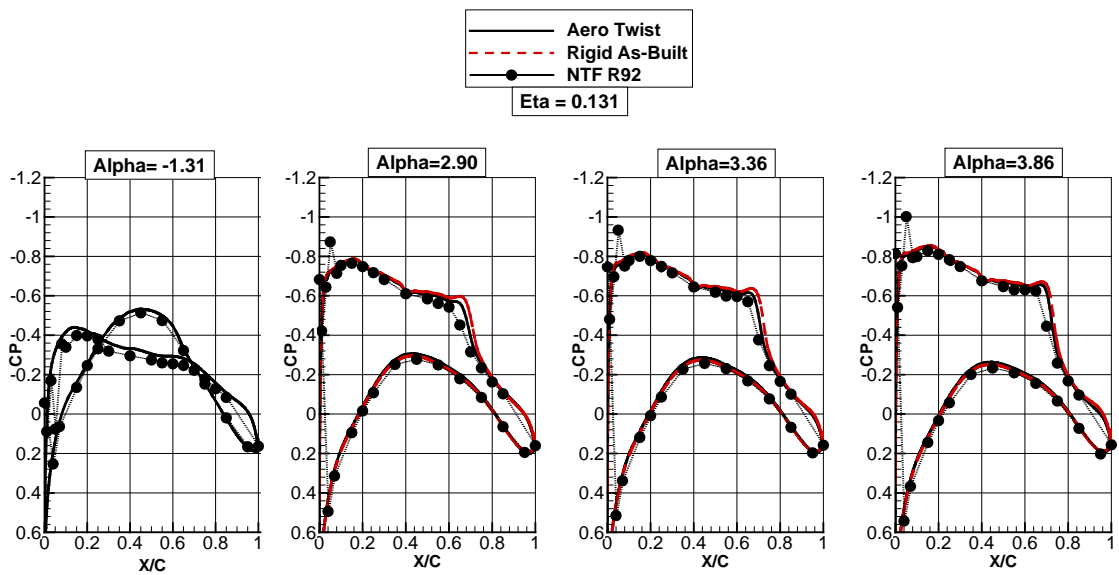


Figure 19. Pressure Distribution Comparisons at  $\eta=0.131$

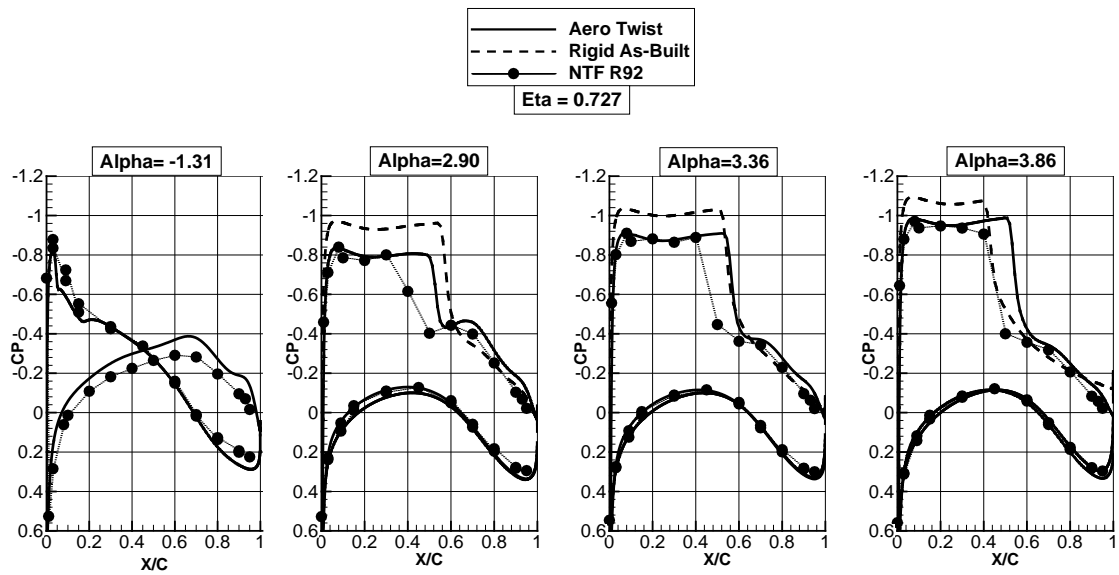


Figure 20. Pressure Distribution Comparisons at eta=0.727

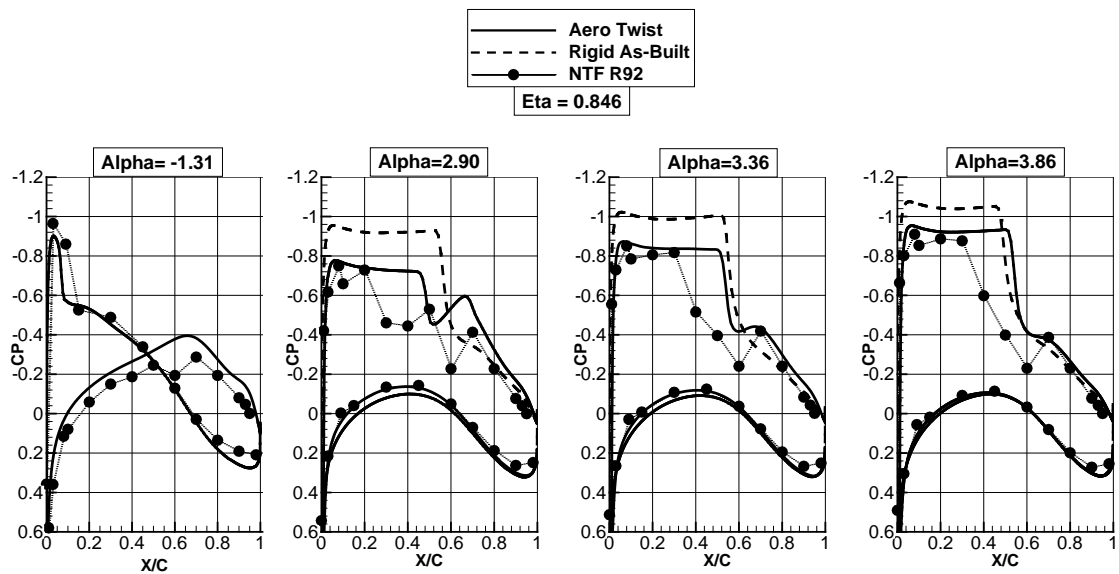


Figure 21. Pressure Distribution Comparisons at eta=0.846

### CRM Wing-Body-Nacelle

The comparisons shown for the CRM Wing-Body-Tail configuration illustrated the importance of including wing aeroelastics in CFD comparisons with wind tunnel data and served to validate the process for quickly including the aeroelastic wing changes at different flow conditions. This process was next applied to the CRM Wing-Body-Nacelle configuration shown in Figure 22. For reference the spanwise section cuts used for the following comparisons are shown in Figure 23. Figure 24 is a plot of the twist angles used for the “Aero Twist” calculations. The twist angles were taken from NASA’s experimental data and applied to the geometry data as described in the introduction. Unfortunately, due to time constraints it was not possible to compute a wide range of flight conditions as was done for the Wing-

Body-Tail configuration. A set of Aero Twist and Rigid As-Built solutions were calculated to compare with experimental results taken an angle of attack = 2.92 degrees.

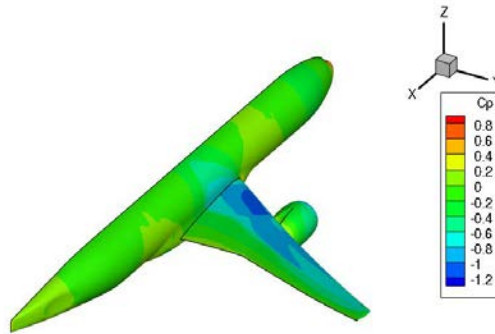


Figure 22. CRM Wing-Body-Nacelle Configuration, Mach=0.85, CL=0.50

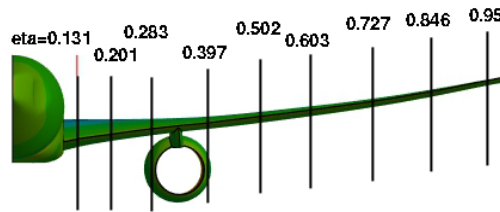


Figure 23. Spanwise Section Cut Locations

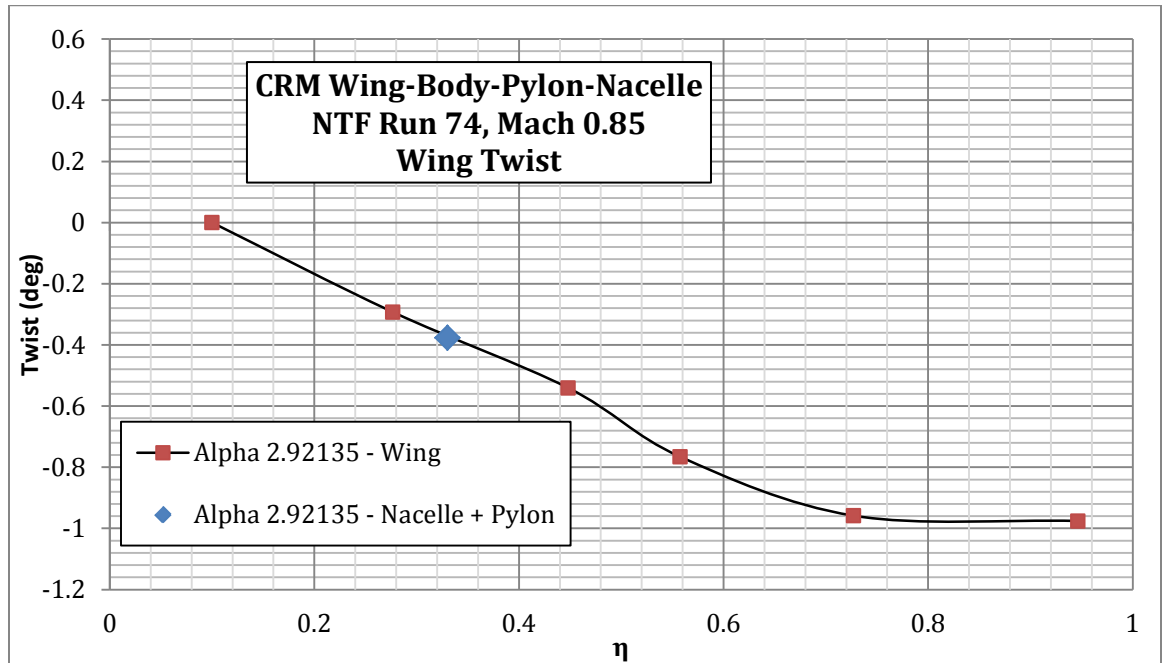


Figure 24. Wing Twist Angles Applied to CRM Wing at specified Angle-of-Attack

The effect of the presence of the nacelle is quite evident as shown in the pressure distributions in Figures 25 and 26. CFD solutions with the Aero Twist for the wing-body-nacelle and wing-body-tail configurations are compared with their respective wind tunnel data.

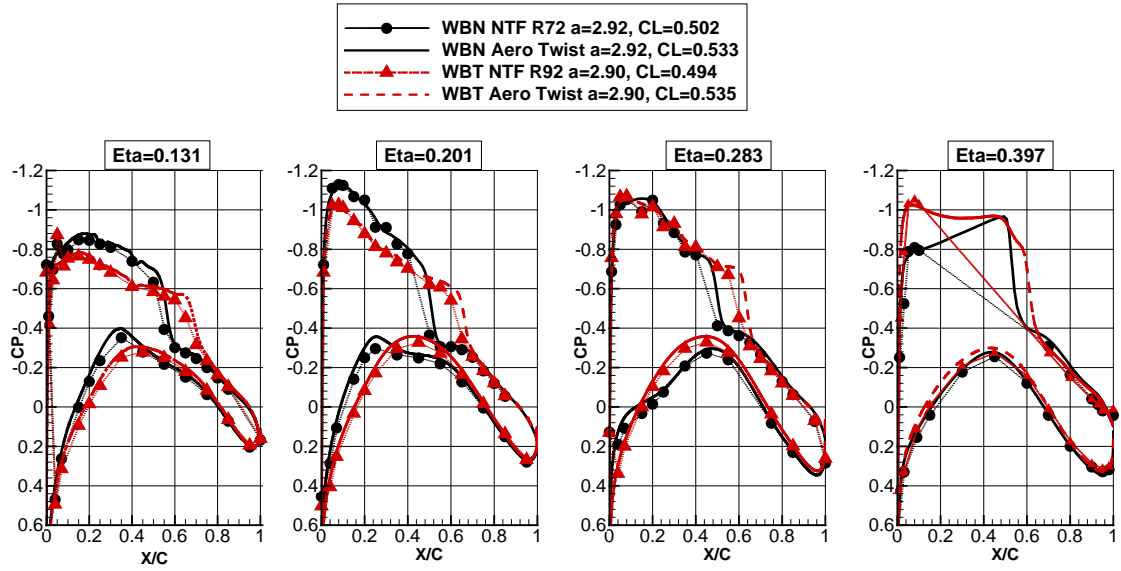


Figure 25. Pressure Distribution Comparisons for the Wing-Body-Nacelle (WBN) and Wing-Body-Tail (WBT) Configurations – Inboard Half

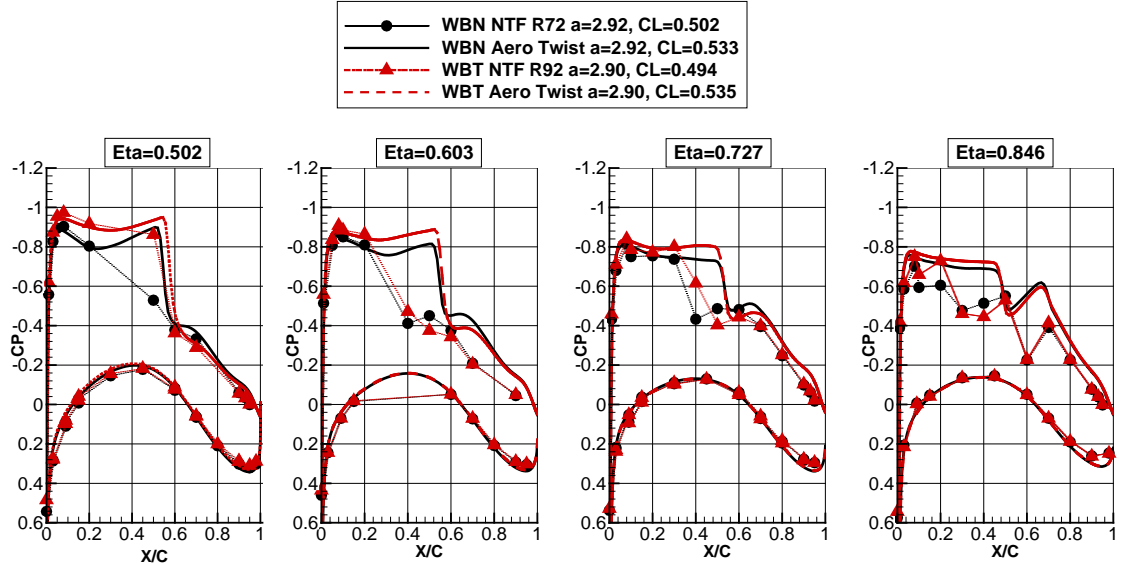


Figure 26. Pressure Distribution Comparisons for the Wing-Body-Nacelle (WBN) and Wing-Body-Tail (WBT) Configurations – Outboard Half

Rigid As-Built and Aero Twist pressure distribution comparisons across the span are shown in Figures 27 and 28. Aero Twist solutions are shown matching angle of attack and lift coefficient. The Rigid As-Built solution matches angle-of-attack. As was seen for the wing-body-tail configuration, the Aero Twist solutions match the “rooftop” pressure levels across the span except for the most outboard station at  $\eta=0.95$  (not shown).

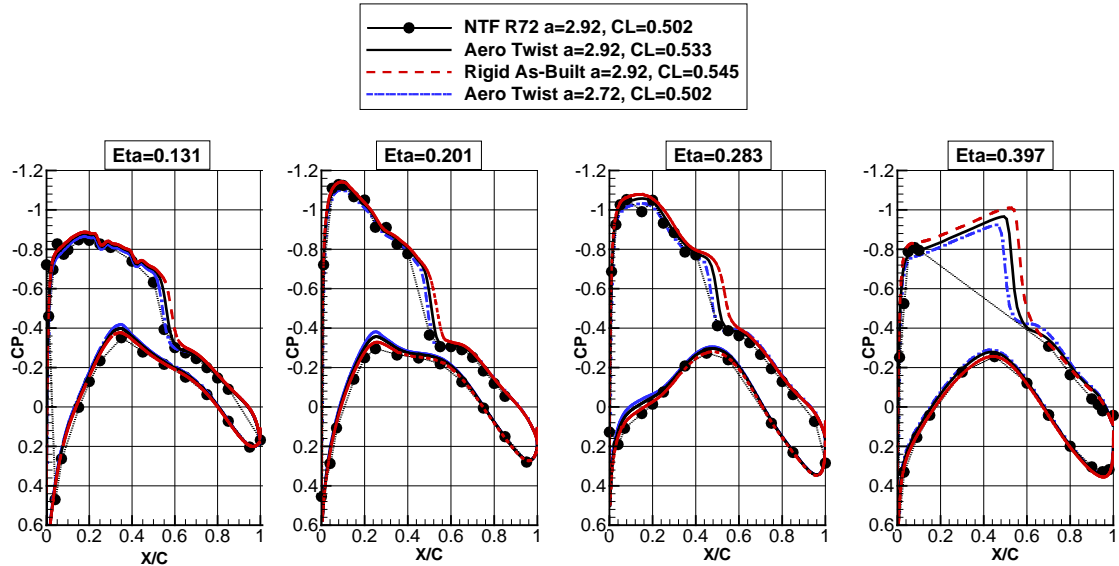


Figure 27. Pressure Distribution Comparisons for the Wing-Body-Nacelle - Inboard Half

**CRM Wing-Body-Nacelle  
Mach=0.85**

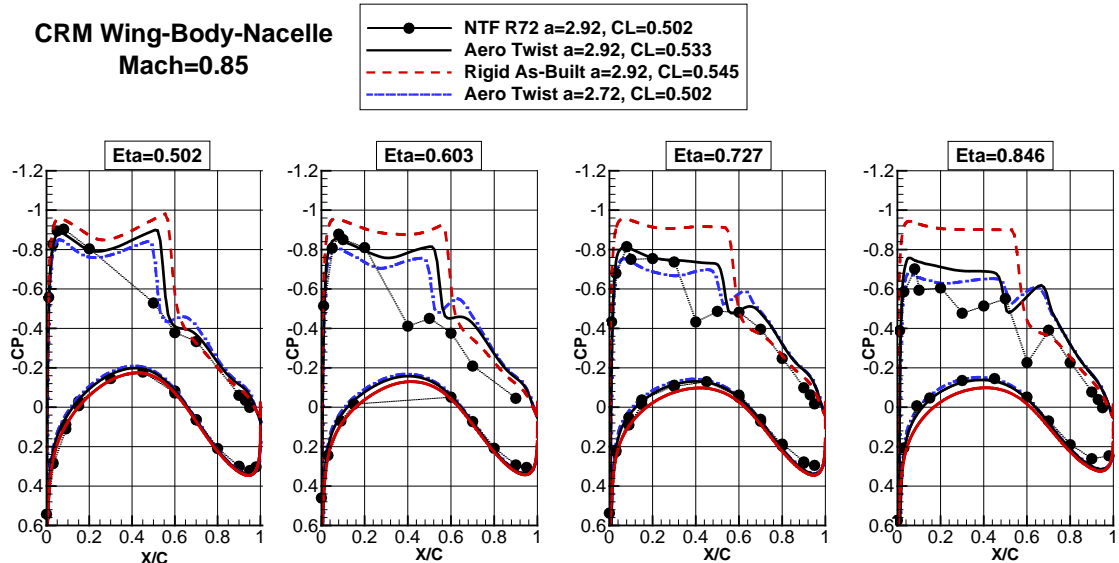


Figure 28. Pressure Distribution Comparisons for the Wing-Body-Nacelle - Outboard Half

We would expect that if a full set of solutions for the wing-body-nacelle configuration were run that we would have seen similar results as those for the wing-body-tail configuration.

#### IV. Concluding Remarks

A process has been developed to easily and reliably incorporate an “aeroelastic” like wing twist distribution into a baseline aircraft configuration. This process has been demonstrated on a “clean wing” configuration as well as one with pylon-mounted engines. The process could also be applied to an aircraft with wing-mounted weapon and/or sensor stores. The twist distribution can be from ‘a priori’ experimental measurements or derived during an iterative aero/structural aeroelastic process.

Whenever a correlation between CFD and experimental data is attempted it should go without saying that the CFD model should match the shape and flight conditions experienced in the experiment. The importance of including wing aeroelastic twist effects in making CFD comparisons with experimental results has been demonstrated. The “twist only” deformation is consistent with a structural “beam” model, and is very adequate for a wind tunnel model in which chordwise structural deformation is negligible. It

should be noted that as significant as the aeroelastics were in these examples, the amount of aeroelastic twist in these cases is typically less than would be seen in most wind tunnel tests. The reason for this is that the wind tunnel model was designed for a much higher dynamic pressure than experienced in the cases shown. A full size airplane structure would experience even greater aeroelastic twist.

#### References:

1. Tinoco, Edward N. "Validation and Minimizing CFD Uncertainty for Commercial Aircraft Applications," AIAA-2008-6902, June 2008.
2. Bussoletti, J. E. "CFD Calibration and Validation: The Challenges of Correlating Computational Model Results With Test Data," AIAA-1994-2542, June 1994.
3. Nathman, J.K., "Subsonic Panel Methods – Second (Order) Thoughts", SAE 985563, Anaheim, CA 1998.
4. Maskew, B., "Prediction of Subsonic Aerodynamic Characteristics: A Case for Low-Order Panel Methods," *J. Aircraft*, Vol. 19, No. 2, February 1982.
5. Nathman, J.K., and Frank, J., "Application of VSAERO to Internal Flows," AIAA Paper 87-2415, Fifth Applied Aerodynamics Conference, Monterey, CA, 1987.
6. Hughes, M., "FSWAVE – A new module for VSAERO to model steady non-linear free surface flows", *Analytical Methods*, 1997.
7. Nathman, J.K., "Improvement of a Panel Method by including Panel Warp", AIAA 2004-0721, Reno, 2004.
8. Nathman, J.K., Induced Drag of High-Aspect Ratio Wings, AIAA 2005-1033, Reno.
9. Nathman, J.K., Hybrid Grid (Structured and Unstructured) Calculations with a Potential-based Panel Method, AIAA 2004-4836, Providence, 2004.
10. Nathman J. K., Potential-Based Panel Method for Oscillatory Motion, AIAA-2006-1255, 2006.
11. *CFD++ User Manual*, Version 6.1. Metacomp Technologies, 2007.
12. Vassberg, J. C., DeHaan, M. A., Rivers, S. M., and Wahls, R. A., "Development of a Common Research Model for Applied CFD Validation Studies," AIAA Paper 2008-6919, 26<sup>th</sup> AIAA Applied Aerodynamics Conference, Hawaii, HI, August 2008.
13. Vassberg, J. C., Tinoco, E. N., Mani, M., Rider, B., Zickuhr, T., Levy, D.W., Brodersen, O., Eisfeld, B., Crippa, S., Wahls, R. A., Morrison, J. H., Mavriplis, D.J., and Murayama, M., "Summary of the Fourth AIAA CFD Drag Prediction Workshop," AIAA Paper 2010-4547, June 2010.
14. Levy, D.W., Laflin, K. R., Vassberg, J. C., Tinoco, E. N., Mani, M., Rider, B., Rumsey, C., Wahls, R. A., Morrison, J. H., Brodersen, O., Crippa, S., Mavriplis, D.J., and Murayama, M., "Summary of Data from the Fifth AIAA CFD Drag Prediction Workshop," AIAA Paper 2012-0046, January 2013.
15. <http://www.beta-cae.gr/conference05.htm>
16. [http://www.beta-cae.gr/events/c5pdf/7B\\_2\\_khandhia.pdf](http://www.beta-cae.gr/events/c5pdf/7B_2_khandhia.pdf)
17. Rivers, M., Hunter, C., and Campbell, R., "Further Investigation of the Support System Effects and Wing Twist on the NASA Common Research Model," AIAA Paper 2012-3209, June 2012.
18. NASA Common Research Model website: <http://commonresearchmodel.larc.nasa.gov>